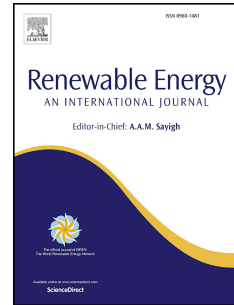


Journal Pre-proof

Finite Blade Functions and Blade Element Optimization for Diffuser-augmented Wind Turbines

Jerson R.P. Vaz, Valery L. Okulov, David H. Wood



PII: S0960-1481(20)31802-4

DOI: <https://doi.org/10.1016/j.renene.2020.11.059>

Reference: RENE 14500

To appear in: *Renewable Energy*

Received Date: 4 April 2020

Revised Date: 11 August 2020

Accepted Date: 12 November 2020

Please cite this article as: Vaz JRP, Okulov VL, Wood DH, Finite Blade Functions and Blade Element Optimization for Diffuser-augmented Wind Turbines, *Renewable Energy*, <https://doi.org/10.1016/j.renene.2020.11.059>.

This is a PDF file of an article that has undergone enhancements after acceptance, such as the addition of a cover page and metadata, and formatting for readability, but it is not yet the definitive version of record. This version will undergo additional copyediting, typesetting and review before it is published in its final form, but we are providing this version to give early visibility of the article. Please note that, during the production process, errors may be discovered which could affect the content, and all legal disclaimers that apply to the journal pertain.

© 2020 Elsevier Ltd. All rights reserved.

Credit Author Statement

Jerson R. P. Vaz

Methodology, Investigation, Writing – Original Draft, Visualization

Valery L. Okulov

Supervision, Project Administration, Funding Acquisition, Writing – Review & Editing

David H. Wood

Conceptualization, Methodology, Writing – Original Draft, Writing – Review & Editing, Visualization

Journal Pre-proof

Finite Blade Functions and Blade Element Optimization for Diffuser-augmented Wind Turbines

Jerson R. P. Vaz^{a,*}, Valery L. Okulov^{b,c}, David H. Wood^d

^a*Faculty of Mechanical Engineering, Institute of Technology, Federal University of Pará - Av. Augusto Correa, N 1 - Belém, PA, 66075-900, Brazil*

^b*Wind Energy Department, DTU, Nils Koppels Alle 403, 2800 Lyngby, Denmark*

^c*Novosibirsk State University, Pirogova Street. 2, 630090, Novosibirsk-90, Russia*

^d*Department of Mechanical and Manufacturing Engineering, Schulich School of Engineering, University of Calgary, Calgary T2N 1N4, Alberta, Canada.*

*Corresponding author

Email address: jerson@ufpa.br (Jerson R. P. Vaz)

Finite Blade Functions and Blade Element Optimization for Diffuser-augmented Wind Turbines

Jerson R. P. Vaz^{a,*}, Valery L. Okulov^{b,c}, David H. Wood^{d,c}

^a*Faculty of Mechanical Engineering, Institute of Technology, Federal University of Pará -
Av. Augusto Correa, N 1 - Belém, PA, 66075-900, Brazil*

^b*Wind Energy Department, DTU, Nils Koppels Alle 403, 2800 Lyngby, Denmark*

^c*Novosibirsk State University, Pirogova Street. 2, 630090, Novosibirsk-90, Russia*

^d*Department of Mechanical and Manufacturing Engineering, Schulich School of
Engineering, University of Calgary, Calgary T2N 1N4, Alberta, Canada.*

Abstract

Placing a diffuser around a wind turbine can increase its power output, but not all mechanisms by which the diffuser alters the aerodynamics have been investigated thoroughly. Here, we concentrate on one such mechanism: the effect of the finite number of blades. In nearly all blade element analyses of wind turbines, finite blade effects are approximated by Prandtl's "tip loss factor" which goes to zero at the blade tip. We argue that this limiting behaviour cannot be correct for the axial velocity in the presence of a diffuser. We provide alternative "finite blade functions" which preserve the finite limit on the axial velocity, but do not alter the conventional limit of zero for the circumferential velocity. In maximizing the power output of a diffuser-augmented wind turbine, the change in the finite blade function for the axial velocity has a large impact on the power-producing region near the tip: it increases both the chord and the power output of an optimized blade. Further, the change appears to make diffuser-augmented turbine power output less sensitive to tip speed ratio than for a bare turbine.

Keywords: Tip loss, DAWT, Diffuser, Blade Element Theory.

*Corresponding author

Email address: `jerson@ufpa.br` (Jerson R. P. Vaz)

27 1. Introduction

28 It is well-known that diffuser augmentation of a wind turbine can increase
 29 the power output, e.g. Jamieson [1]. This increase is proportional to the flow
 30 rate of air induced through the rotor by the diffuser, e.g. Hansen et al.
 31 [2], showing the importance of the diffuser design, a subject that has been
 32 studied extensively, e.g. Hjort & Larsen [3]. No large diffuser-augmented
 33 wind turbines (DAWTs) have been commercially successful, but there is a
 34 strong potential for small DAWTs in urban areas, where the wind conditions
 35 and the specific needs for safety favour the concept, e.g. Anup et al. [4] and
 36 Dilimulati et al. [5]. Diffuser-augmented hydrokinetic turbines (DAHKTs)
 37 also have promise for rivers and tidal flows, e.g. Silva et al. [6]. Even for
 38 these applications, however, there is some doubt as to whether the increase
 39 in total mass, size, and cost over a bare turbine is beneficial, e.g. Lubitz &
 40 Shomer [7]. It follows that DAWTs need to be aggressively optimized.

41 Adding a diffuser is simple in concept, but often complex to analyze,
 42 even when using basic blade element momentum theory (BEMT), the main
 43 workhorse for the study of bare turbines, e.g. Hansen [8]. The diffuser can
 44 be modeled using computational fluid dynamics (CFD), e.g. [3] and Kesby
 45 et al. [9], and, clearly, its performance is influenced by interaction with the
 46 blades. If CFD is not used, it is often assumed that the diffuser is perfectly
 47 efficient, although methods to include finite efficiency have been available for
 48 a long time, e.g. Fletcher [10], who ignored diffuser thrust, and Vaz & Wood
 49 [11] who included it.

50 This paper concentrates on an aspect of BEMT for DAWTs that has
 51 received little attention: the accounting for the finite number of blades, N .
 52 This is routinely done in BEMT for any turbine by using Prandtl's "tip
 53 loss factor", F_P , in the form developed by Glauert [12], see also Sørensen
 54 [13]. Finite N causes the induced velocities at the blades to differ from the
 55 streamtube averages. Following the paragraph before Eq. (5.3) in Glauert
 56 [12], the axial, F_u , and circumferential, F_w , "finite blade functions" can be
 57 written in terms of the induced axial and circumferential velocities, a , and
 58 a' respectively, as

$$F_u = a/a_b \quad \text{and} \quad F_w = a'/a'_b, \quad (1)$$

59 where the subscript "b" denotes a value at the blade and a symbol without
 60 "b" denotes a streamtube average. The calculation of the induced velocities is
 61 described in Section 3. The standard approximation is $F_u = F_w = F_P$, where

62 $F_P \leq 1$. For bare turbines, a difference between F_u and F_w was considered,
 63 but not used, by Shen et al. [14], while Wimhurst & Willden [15] determined
 64 F_u and F_w using a three-dimensional computational simulation. As $N \rightarrow \infty$,
 65 $F_P, F_u, F_w \rightarrow 1$ because there is no difference between a and a_b , or between
 66 a' and a'_b , for an actuator disk. Further, F_P goes to zero at the blade tip and
 67 has a strong influence on the torque and thrust acting on the blade elements
 68 in the outer part of a blade.

69 We believe that “tip loss factor” is not a good name for F_u and F_w , and
 70 will continue to use the more general “finite blade functions” which covers
 71 the following situations. If the blades have “pre-bend” or are “coned”, that is
 72 they do not lie entirely in the radial plane, then the velocity at each element
 73 is influenced by the bound circulation of every other element, e.g. Wood
 74 [16]. If the blades are unequally loaded, due to wind shear or yaw, there are
 75 “cascade” effects from the other blade elements at the same radius, Wood
 76 [17]. These cases, which cannot be modeled by F_P , are not considered here
 77 because F_P has an even more important deficiency for DAWTs: it is zero
 78 at the tip for both the axial and circumferential flow. A diffuser, however,
 79 *induces* an axial velocity through the rotor that may vary radially, but not
 80 circumferentially. This situation does not correspond to the idealized vortex
 81 sheet model that was probably used by Prandtl to derive his tip loss formula,
 82 see Glauert [12] and Sørensen [13]. Since all induced velocities must be
 83 included in Eq. (1), F_u cannot be zero at the blade tip in a DAWT, but
 84 F_w can be zero. The tip region of a DAWT has some similarities to the tip
 85 regions of a gas turbine which have much more complex flow, but the presence
 86 of the end wall prevents complete unloading at the tip. Figure 11 of Passman
 87 et al. [18], for example, shows the blade loading for a simplified blade model
 88 at 95% span is not significantly reduced from the value at midspan. The
 89 secondary vortex formation that is associated with tip effects must occur for
 90 DAWTs of sufficiently small tip clearance but we are unaware of any detailed
 91 study of them. Ironically, these tip effects are not captured by the “tip loss
 92 factor”. The present analysis using a simple model for F_u and F_w can be
 93 viewed as a small step in the direction of improved tip modeling.

94 We consider a DAWT with the simplest configuration of straight, un-
 95 coned, equally-loaded blades, because then only the trailing vorticity can
 96 change the blade element velocities from the streamtube averages. We de-
 97 velop the analysis of Wood & Okulov [16] and [19] for bare turbines. They
 98 used Okulov’s [20] approximations to the Kawada-Hardin (KH) equations
 99 for the velocity field induced by a semi-infinite helical vortex of constant ra-

100 dius and pitch, see Fukumoto et al. [21]. The equations are applied to the
 101 vortices trailing from the junctions of all blade elements, as well as the hub
 102 and tip, to compute the velocities at the centre of each element. Because
 103 of the restriction to vortices of constant radius and pitch, the KH equations
 104 are undoubtedly simplistic. In principle, the resulting finite blade functions
 105 are less accurate than could be obtained numerically, e.g. [15]. On the other
 106 hand the equations are analytic and are straightforward to combine with a
 107 BEMT computation.

108 The KH equations and Okulov’s approximations have the important char-
 109 acteristic that [16] and [19] called “Kawada cancellation”; the velocity varia-
 110 tions in the circumferential direction due to N equally-spaced helical vortices
 111 of the same strength, Γ , tend to zero as $N \rightarrow \infty$ so that F_u and F_w tend to
 112 unity in the same limit. The results in [16] and [19] show that F_u and F_w
 113 increasingly differ from F_P as tip speed ratio, λ is reduced. Although it is
 114 not the primary reason to study finite blade functions for DAWTs, we note
 115 that their typical λ is lower than for bare turbines.

116 In this paper, we describe for the first time the determination of F_u and
 117 F_w for a DAWT, and their use in a blade element analysis to determine
 118 thrust and power. The BEMT method of Vaz & Wood [11], which includes
 119 the diffuser efficiency and thrust, is modified by replacing F_P by F_u or F_w
 120 where appropriate. We also adjust their expression for the axial velocity at
 121 the rotor. The next Section summarizes vortex theory for DAWTs. The
 122 following Section describes the integration of F_u and F_w into a BEMT opti-
 123 mization. Section 4 details the calculation of the finite blade functions, and
 124 then Section 5 describes the simulated DAWT. Section 6 gives the results.
 125 The last Section, 7, contains the conclusions.

126 2. Vortex Theory for DAWTs

127 Fig. 1 depicts a DAWT with $N = 2$; this number is used in the figure
 128 only for convenience as the following analysis holds for any N . A vortex sheet
 129 continuously sheds from each blade with an induced axial velocity of w . V_0
 130 is the freestream velocity, and Ω is the angular speed of the rotor. In the
 131 absence of the rotor, the diffuser induces an extra flow whose axial velocity
 132 at the rotor position is V_d , which may be a function of radius, r , but not
 133 of the circumferential co-ordinate. When the turbine is operating, the axial
 134 velocity at the rotor is V_1 . Therefore, the diffuser maximizes F_u at the tip
 135 relative to F_p . V_1 , however, will differ from its value when there is no rotor,

136 $V_0 + V_d$, in a manner similar to the difference between V_0 and the velocity of
 137 the rotor of a bare turbine.

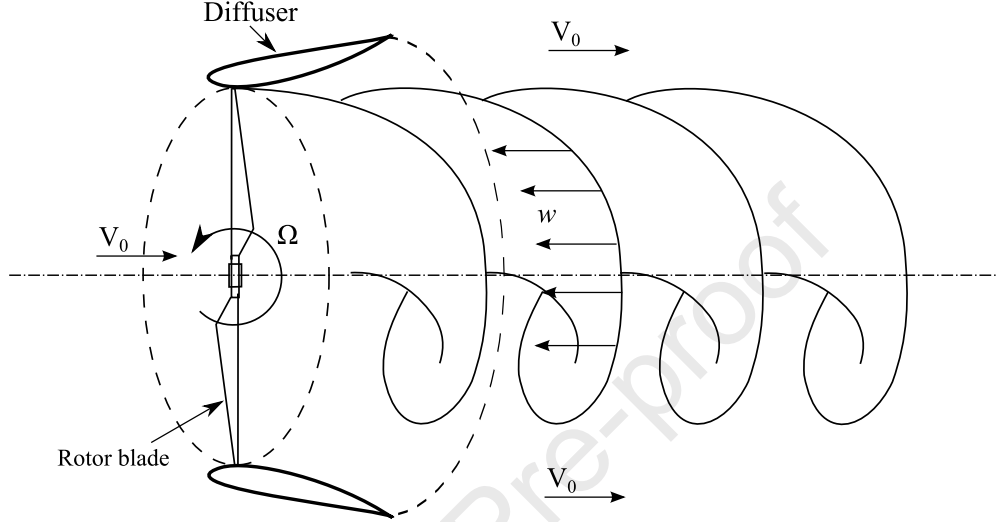


Figure 1: Simplified illustration of the helical surface of an ideal wake of a diffuser-augmented wind turbine, adapted from Okulov & Sørensen [22].

138 The following exposition of geometric aspects of vortex theory for a
 139 DAWT is a straightforward development of that in Okulov & Sørensen [22]
 140 for a bare turbine. The major addition is V_d , which may be calculated simply
 141 by applying the momentum equation to the control volume shown in Fig. 2
 142 for an empty diffuser. Hence, the energy balance downstream of the diffuser
 143 exit, denoting the losses as ΔH , gives:

$$1 = c_{p3} + \beta^2 \left(\frac{V_1}{V_0} \right)^2 + \frac{\Delta H}{\frac{1}{2}\rho V_0^2}, \quad (2)$$

144 where β is the diffuser area ratio, and the pressure coefficient, c_{p3} , at the
 145 diffuser outlet is

$$c_{p3} = \frac{p_3 - p_0}{\frac{1}{2}\rho V_0^2}, \quad (3)$$

146 in which p_0 is the static pressure in the external flow, [11]. Introducing the

147 diffuser efficiency, η_d , the losses are computed through

$$\Delta H = \frac{1}{2} \rho V_0^2 \left(\frac{V_1}{V_0} \right)^2 (1 - \eta_d) (1 - \beta^2), \quad (4)$$

148 so that $\Delta H = 0$ if $\eta_d = 1$. The total velocity at the rotor plane of the empty
149 diffuser is $V_0 + V_d$, yielding in normalized form:

$$v_d = \frac{V_d}{V_0} = \sqrt{\frac{1 - c_{p3}}{\beta^2 + (1 - \eta_d) (1 - \beta^2)}} - 1. \quad (5)$$

150 Thus V_d is independent of r but dependent on the pressure coefficient at the
151 diffuser exit, area ratio, and the diffuser efficiency.

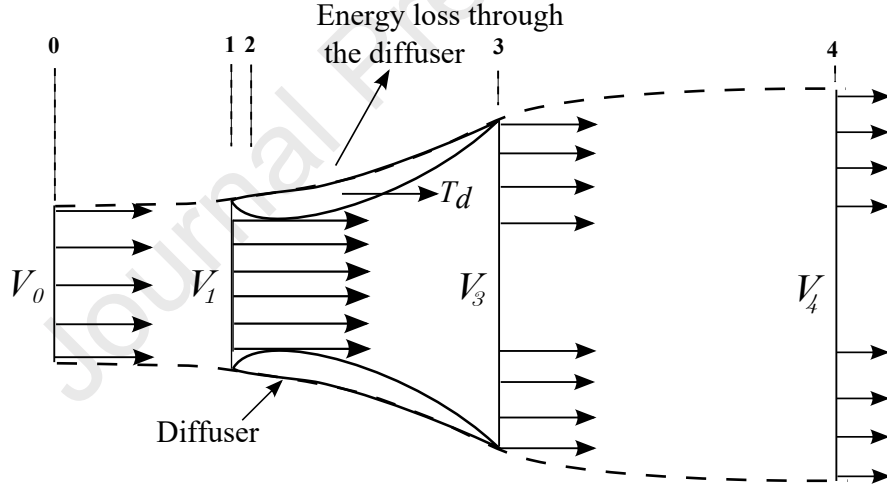


Figure 2: Control volume of an empty diffuser.

152 According to the velocity diagram in Fig. 3, the total axial velocity of
153 the vortex sheet is $V_0 - w + V_d = V_1 - w$. V_d influences the pitch, p , of the
154 helicoidal wake because the dimensionless form of $p(r)$ is

$$\frac{p}{r} = \tan \phi = \frac{V_0 - w + V_d}{\Omega r}, \quad (6)$$

155 where ϕ is the angle between the vortex sheet and the rotor plane defined in

156 Fig. 3. For completeness, we note that p can also be written as

$$p = \frac{1}{\tilde{\lambda}} (1 - \tilde{w}), \quad (7)$$

157 where the “modified tip speed ratio” $\tilde{\lambda} = \Omega R/V_1$ and $\tilde{w} = w/V_1$. This
158 equation is not used in the present analysis.

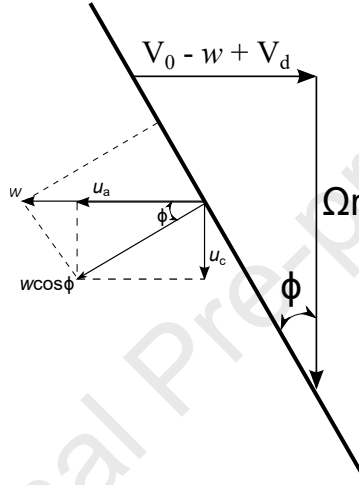


Figure 3: Velocity diagram for the vortex sheet of a DAWT, adapted from Okulov & Sørensen [22].

159 The axial and circumferential velocity components induced by the sheet
160 are the same as for a bare turbine. As given by Okulov & Sørensen [22], the
161 axial velocity, u_a , induced by the helix is

$$u_a = w \cos^2 \phi = \frac{wr^2}{p^2 + r^2}. \quad (8)$$

162 Similarly, the equation for the circumferential induced velocity, u_c , is

$$u_c = w \sin \phi \cos \phi = \frac{wrp}{p^2 + r^2}. \quad (9)$$

163 Extending Eq. (24) of Okulov & Sørensen [22], ϕ is also given by

$$\tan \phi = \frac{V_0 - u_a + V_d}{\Omega r + u_c} = \frac{V_1 - u_a}{\Omega r + u_c}. \quad (10)$$

164 The bound circulation of each element, Γ , needed later to determine u_a

165 and u_c , comes from the torque acting on the blade element:

$$\Gamma = \frac{1}{2} U_T c C_l \left(1 - \frac{C_d}{C_l \tan \phi} \right), \quad (11)$$

166 where c is the chord, C_l and C_d are the lift and drag coefficients, respectively,
167 and the total blade element velocity is

$$U_T = \sqrt{(V_1 - u_{a,b})^2 + (\Omega r + u_{c,b})^2}, \quad (12)$$

168 where subscript “ b ” indicates, as before, the velocities are at the blades and
169 not the streamtube averages.

170 For the development of BEMT for DAWTs, the important results of this
171 section are Eqs. (11) and (12). p will also be shown to be dynamically
172 important for reasons directly connected to the vortex geometry. For bare
173 turbines, w is usually taken as a parameter that can be optimized to maxi-
174 mized turbine output power, e.g. [16], [19], and [22]. It has been found that
175 $w \rightarrow 1/3$ as $\lambda \rightarrow \infty$, that is, the vortex sheet moves with the velocity of the
176 remainder of the wake.

177 3. Blade Element Theory for DAWTs

178 The inclusion of F_u and F_w in the blade element equations for DAWTs is
179 straightforward. Vaz & Wood [11] derived these equations, but they used F_P .
180 All that is necessary here is to substitute F_u for F_P in the thrust equation
181 and F_w for F_P in the torque equation. Eq. (16) of [11] gives the elemental
182 thrust, C_T , and torque coefficients, C_M , on the blade elements intersecting
183 an annular control volume at radius r , which hereinafter is normalized by R ,
184 as

$$\frac{dC_T}{dr} + \frac{dC_{Td}}{dr} = 4\varepsilon_1 (1 - \varepsilon_4) r, \quad (13)$$

185 where C_{Td} is the thrust coefficient of the diffuser, and ε_4 is the streamtube
186 average diffuser exit velocity given by Eq. (18) of [11], and

$$\frac{dC_M}{dr} = 4\varepsilon_1 u_c r^2, \quad (14)$$

187 with the normalized velocity at the rotor plane ε_1 given by

$$\varepsilon_1 = V_1 (1 - a) / V_0 = (1 + v_d)(1 - a), \quad (15)$$

188 where a , the streamtube average axial induction factor, is defined in the same
 189 way as for a bare turbine, as V_1 would be the velocity at the location of the
 190 rotor if it was removed. After the change from using F_P to F_u and F_w , Eq.
 191 (15) is the main difference from the analysis of [11]. ε_4 is given by

$$\varepsilon_4 = \varepsilon_{1,b} - \sqrt{(1 - \varepsilon_{1,b})^2 + C_{Td} - \varepsilon_{1,b}^2(1 - \beta^2)(1 - \eta_d)}. \quad (16)$$

192 with $\varepsilon_{1,b} = (1 + v_d)(1 - a_b F_u)$, and F_u replacing F_P . Combining Eqs. (13)
 193 and (16) gives

$$\frac{dC_T}{dr} + \frac{dC_{Td}}{dr} = 4\varepsilon_1 \left[1 - \varepsilon_{1,b} + \sqrt{(1 - \varepsilon_{1,b})^2 + C_{Td} - \varepsilon_{1,b}^2(1 - \beta^2)(1 - \eta_d)} \right] r, \quad (17)$$

194 which is the new form of Eq. (19) of [11], and

$$\frac{dC_M}{dr} = 8a'_b F_w \lambda (1 + v_d) (1 - a_b) r^3, \quad (18)$$

195 where $\lambda = \Omega R/V_0$ is the conventional tip speed ratio. This is the new form
 196 of Eq. (20) of [11]. Note that for a bare turbine ($\eta_d = 1$ and $C_{Td} = 0$),
 197 Eq (17) reduces to Eq. (5) of Wood & Okulov [19], while Eq. (18) matches
 198 their (6), when the missing λr is included in the latter. The element power
 199 is obtained from

$$dP = \Omega dM = 4\rho a'_b F_w V_0 (1 + v_d) (1 - a_b) \Omega^2 r^3 \pi dr. \quad (19)$$

200 By integrating this expression across the rotor, the power coefficient is given
 201 by

$$C_P = \frac{P}{\frac{1}{2}\rho A V_0^3} = \frac{8(1 + v_d)}{\lambda^2} \int_0^\lambda a'_b F_w (1 - a_b) x^3 dx, \quad (20)$$

202 where $x = \Omega r/V_0$ is the local-speed ratio.

203 From the lift and drag acting on an element, the contributions to the
 204 thrust and torque coefficients are

$$\frac{dC_T}{dr} = 2 [(1 + v_d) (1 - a_b)]^2 \frac{\sigma C_n r}{\sin^2 \phi} \quad (21)$$

205 and

$$\frac{dC_M}{dr} = 2 \frac{(1 + v_d)(1 - a_b)(1 + a'_b) \sigma C_t \lambda r^3}{\sin \phi \cos \phi}, \quad (22)$$

206 where $\sigma = Nc/(2\pi r)$ is the local solidity. The elemental normal and tan-
 207 gential force coefficients C_n and C_t , respectively, at any r have the same
 208 definition as for a bare turbine, see Eqs. (16) and (17) of Vaz & Wood [26].
 209 C_n and C_t are a convenient way of using the element lift and drag coefficients.
 210 The flow angle, ϕ , is given by Eq. (25) of Vaz & Wood [11]. An extended
 211 formulation for the axial and tangential flow velocities can be obtained by
 212 combining Eqs. (17) and (18) with Eqs. (21) and (22) respectively, yielding

$$1 - \varepsilon_{1,b} + \sqrt{(1 - \varepsilon_{1,b})^2 + C_{Td} - \varepsilon_{1,b}^2(1 - \beta^2)(1 - \eta_d)} - \frac{1}{4\varepsilon_{1r}} \frac{dC_{Td}}{dr} = \frac{\varepsilon_1 \sigma C_n}{2 \sin^2 \phi} \quad (23)$$

213 and

$$\frac{a'_b}{1 + a'_b} = \frac{\sigma C_t}{4F_w \sin \phi \cos \phi}. \quad (24)$$

214 Section 4 describes the calculation of F_u and F_w .

215 3.1. Blade Element Optimization for DAWTs

216 The optimum value of ε_{1opt} is determined by maximizing C_P according
 217 to the description in [11], which is done using

$$6\varepsilon_{1opt}^3 [\beta^2(1 - \eta_d) + \eta_d] - C_{Td}\Delta + 4\varepsilon_{1opt}(1 + C_{Td} + \Delta) - 2\varepsilon_{1opt}^2(5 + 3\Delta) = 0, \quad (25)$$

218 where

$$\Delta = \sqrt{1 + C_{Td} + \varepsilon_{1opt} \{-2 + \varepsilon_{1opt} [\beta^2(1 - \eta_d) + \eta_d]\}}. \quad (26)$$

219 which are Eqs. (29) and (3) of [11]. Once ε_{1opt} is obtained, the optimized a_{opt}
 220 may be easily calculated through $a_{bopt} = 1 - \varepsilon_{1opt}$. a' as a function of ε_{1opt} is
 221 found using conservation of energy, resulting in optimum element power:

$$dP_{opt} = \frac{1}{2} \rho V_0^3 [\varepsilon_{1opt}(1 - \varepsilon_{4opt}^2) - \varepsilon_{1opt}^2(1 - \beta^2)(1 - \eta_d)] dA. \quad (27)$$

222 Also, applying the angular momentum equation at a blade section,

$$dP_{opt} = 2\rho V_0 a'_b \varepsilon_{1opt} \Omega^2 r^2 dA. \quad (28)$$

223 Equating (27) and (28) gives

$$a'_{bopt} = \frac{2\varepsilon_{1opt}(1 - \varepsilon_{4opt}) - C_{Td}}{4x^2}, \quad (29)$$

224 with ε_{4opt} given by

$$\varepsilon_{4opt} = \varepsilon_{1opt} - \sqrt{(1 - \varepsilon_{1opt})^2 + C_{Td} - \varepsilon_{1opt}^2(1 - \beta^2)(1 - \eta_d)}. \quad (30)$$

225 In this case, F_u is included in ε_{4opt} through $\varepsilon_{1opt} = (1 + v_d)(1 - a_{bopt}F_u)$.

226 Hence, the optimum flow angle, ϕ_{opt} , can be determined through

$$\phi_{opt} = \tan^{-1} \left[\frac{(1 + v_d)(1 - a_{bopt})}{x(1 + a'_{bopt})} \right]. \quad (31)$$

227 To calculate the optimum twist angle, θ_{opt} , and chord, c_{opt} , the following
228 expressions are used:

$$\theta_{opt} = \phi_{opt} - \alpha_{opt} \quad (32)$$

229 and

$$c_{opt} = 4\pi r (1 - \varepsilon_{4opt}) \frac{\sin^2(\phi)}{NC_n \varepsilon_{1opt}}. \quad (33)$$

230 Note that Eq. (33) comes directly from (21).

231 4. Calculation of the Finite Blade Functions for DAWTs

232 The procedure developed in [16], [17], and [19] calculates the mean in-
233 duced velocities from their simple dependence on Γ , given by Eq. (11). The
234 major difference is that Γ and $p(r)$ are calculated through BEMT expres-
235 sions, which are dependent on η_d , β , and C_{Td} . Thus, for the streamtube
236 whose centre is at radius r , a and a' in Eq. (1) are given by

$$a = \frac{N\Gamma}{4\pi p V_0} \quad \text{and} \quad a' = \frac{W}{\Omega r} = \frac{N\Gamma}{4\Omega\pi r^2}, \quad (34)$$

237 where W is the induced circumferential velocity. Note that the terms involv-
 238 ing Γ are consistent with Eqs. (8) and (9). Further

$$a_b = a + \delta a \quad \text{and} \quad a'_b = a' + \delta a', \quad (35)$$

239 where δa and $\delta a'$, the difference between the values at the blades and the
 240 means, are due entirely to the trailing vortices. They are found using Okulov's
 241 approximation to the KH equations. The BEMT implementation of these
 242 equations, including the use of Kawada cancellation, is described in Section
 243 2 of Wood [16], especially Eqs. (6) and (7), so the details will be omitted
 244 here. The only significant alteration to that method is including η_d , β , and
 245 C_{Td} in F_u and F_w through Eqs. (11) and (36). The finite blade functions
 246 are then computed using Eq. (1). The presence of η_d , β , and C_{Td} in the cal-
 247 culation of U , W , and the values at the blade requires F_u and F_w to remain
 248 finite at the blade tip unless $v_d = 0$ for a bare turbine.

249 The final requirement is a value of p . Following [17], [19], and [16], this
 250 is given by

$$p = dC_M/dC_T, \quad (36)$$

251 and so it is easily obtained from Eqs. (21) and (22). The use of Eq. (36)
 252 removes the need to compute an optimum w for the vortex sheet in Eq. (7).

253 The iterative algorithm for the calculation of optimum chord and twist
 254 angle, starting at the tip, is described below, using the following as input:
 255 r , η_d , β , C_{Td} , $C_L(\alpha_{opt})$, $C_D(\alpha_{opt})$ and V_0 for a given λ . Note that there are
 256 two iterations over N_s , the number of blade sections: the first is the blade
 257 element calculations and the second is to determine F_u and F_w . Conventional
 258 BEMT algorithms use only the first. For all calculations in this paper, $N_s =$
 259 30.

Set initial values: $F_u = F_w = 1$;

while $error > TOL$ **do**

for $i = 1$ to N_s **do**

$iter = iter + 1$;

 Compute $a_{b_{opt}}$, making $a_{b_{opt}} = 1 - \varepsilon_{1_{opt}}$ using Eq. (25), and $a'_{b_{opt}}$ using Eq. (29);

 Compute ϕ_{opt} using Eq. (31);

 Compute $C_n = C_L(\alpha_{opt}) \cos \phi_{opt} + C_D(\alpha_{opt}) \sin \phi_{opt}$ and $C_t = C_L(\alpha_{opt}) \sin \phi_{opt} - C_D(\alpha_{opt}) \cos \phi_{opt}$, respectively, where α_{opt} is obtained from maximum C_L/C_D ;

 Compute θ_{opt} and c_{opt} , using Eqs. (32) and (33), respectively;

 Compute U_T using Eq. (12);

 Compute dC_T and dC_M using Eqs. (17) and (18), respectively;

end for

 Compute $C_p = \lambda \sum dC_M$;

 Compute Γ using Eq. (11);

 Compute p using Eq. (36);

for $i = 1$ to N_s **do**

 Compute new $F_u = a/a_{b_{opt}}$ and new $F_w = a'/a'_{b_{opt}}$ using Eq. (34). It is important to note that F_u and F_w are implemented in the algorithm through $\varepsilon_{1,b} = (1 + v_d)(1 - a_b F_u)$, and F_w in Eq. (18);

end for

 Compute $error = |C_p^{iter+1} - C_p^{iter}|$.

end while

Compute blade geometry.

260 5. The Simulated Diffuser-Augmented Wind Turbine

261 We consider the diffuser of Hansen et al. [2], made by deforming the
 262 NACA 0015 airfoil, for which the parameters are shown in Table 1. To
 263 evaluate F_u and F_w , it is necessary to find v_d through Eq. (5). The difference
 264 for v_d between the present model and the CFD results of Hansen et al. [2]
 265 is about 0.012%, for the same values for β , η_d , and c_{p3} . This implies the
 266 validity of Eq. (5) for the induced velocity, v_d .

Table 1: Comparison between the proposed model and CFD [2].

	β	η_d	c_{p3}	v_d
Hansen et al. [2]	0.54	0.83	-0.38	0.83
Present work, Eq. (5)	0.54	0.83	-0.38	0.8301

267 A DAWT optimization was done for $N = 3$ using the symmetrical NACA
 268 0012 airfoil, with C_l and C_d obtained experimentally by Sheldahl and Klimas
 269 [50]. The main parameters for the optimization procedure are shown in Table
 270 2. The NACA 0012 is one of the most studied airfoils, so there are extensive
 271 experimental data available in the literature. The NACA 0012 airfoil is
 272 used here for convenience: it is not the objective of this work to evaluate
 273 the effect of the airfoil on DAWT performance. The angle of attack of 8°
 274 gave the maximum C_l/C_d around 44, for a Reynolds number of 1.6×10^5 .
 275 The parameters listed in Table 2 are input data for the present procedure,
 276 through which the blade is designed. In the optimization, F_u and F_w are
 277 calculated from the contribution to the blade element velocities induced by
 278 the vortices trailing from each element junctions, as well as the hub and the
 279 tip.

Table 2: Design parameters used in the simulation of the DAWT.

Parameters	Values
Turbine Diameter (D)	2.0 m
Hub Diameter (d)	0.2 m
Lift coefficient (C_l)	0.8274
Drag coefficient (C_d)	0.0185
Optimum angle of attack (α)	8°
Number of blades (N)	3
Tip-Speed Ratio (λ)	2.0 and 7.0
Air density (ρ) at 25°C	1.2 kg/m^3

280 6. Results and Discussion

281 Fig. 4 shows the behavior of the finite blade functions, F_u , F_w , and F_p at
 282 $\lambda = 2.0$. For $v_d = 0.0$ (Fig. 4a), indicating that for a bare turbine, F_u and
 283 F_w are coincident, as they must be if p is constant, which is an optimality
 284 condition, e.g. Wood [16]. As in previous analyses, e.g. Wood [16], the

285 calculated F_u and F_w exceed unity near the hub. It is not clear whether
 286 this behaviour is correct, but, fortunately, the contribution to the power and
 287 thrust from the hub region is small. The finite blade functions, therefore,
 288 were constrained so that $F_u \leq 1$ and $F_w \leq 1$ along the entire blade. Thus,
 289 near the hub, F_u and F_w remain equal to unity with and without the diffuser,
 290 Fig. 4. Over the whole blade, F_u and F_w change substantially compared to
 291 F_p when there is a diffuser as shown in Fig. 4b. Also, $F_u > F_w$ close to the
 292 tip, where v_d becomes the dominant contribution to the streamtube average
 293 as well as the velocity at the blades. Such a behavior does not occur for F_p .
 294 Fig. 5 shows F_u , F_w , and F_p for $\lambda = 7.0$. Note that F_u , F_w and F_p are more
 295 nearly equal for the bare turbine (Fig. 5a). This occurs because F_p becomes
 296 more accurate as λ increases, as pointed out in [51]. For $v_d = 0.82$, indicating
 297 a DAWT with $C_{T,d} = 0.8$, F_u remains equals to F_w at this higher λ , but larger
 298 than F_p , as shown in Fig. 5b. As shown by the insert in Fig. 5b, $F_u \approx F_w$
 299 at the tip, despite the diffuser contributing to the axial flow only. We interpret
 300 this result to mean that the blade bound circulation stays positive due to v_d
 301 and this causes F_w to be non-zero. The difference between F_p and F_u and F_w
 302 is further reflected in Fig. 6, which shows Γ , with and without the diffuser.
 303 Clearly, the diffuser increases the circulation along the entire blade, making
 304 $F_u = F_w > F_p$ when λ increases. This increase in circulation increases the
 305 power extraction, but it also may increase the effect of cavitation. This is
 306 a very important phenomenon for hydrokinetic turbine blade optimization,
 307 which is intensified when operating at low λ .

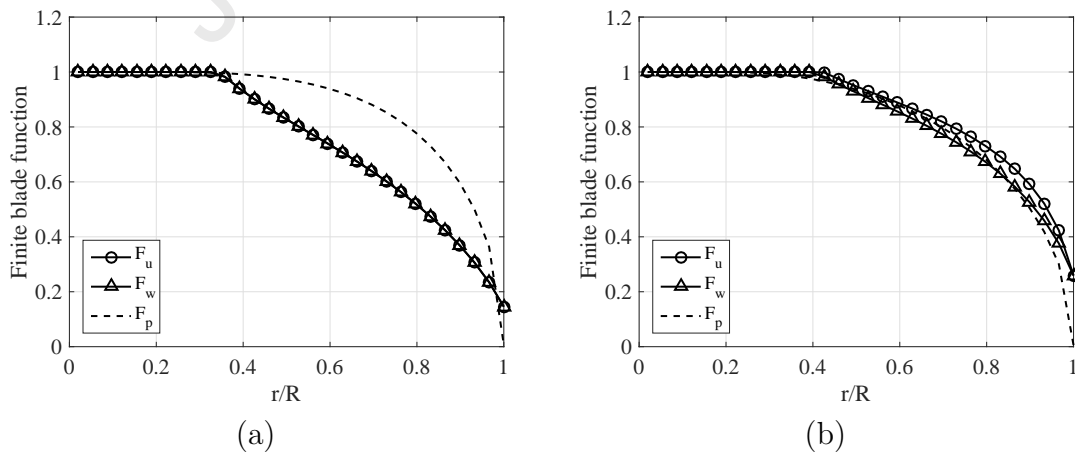
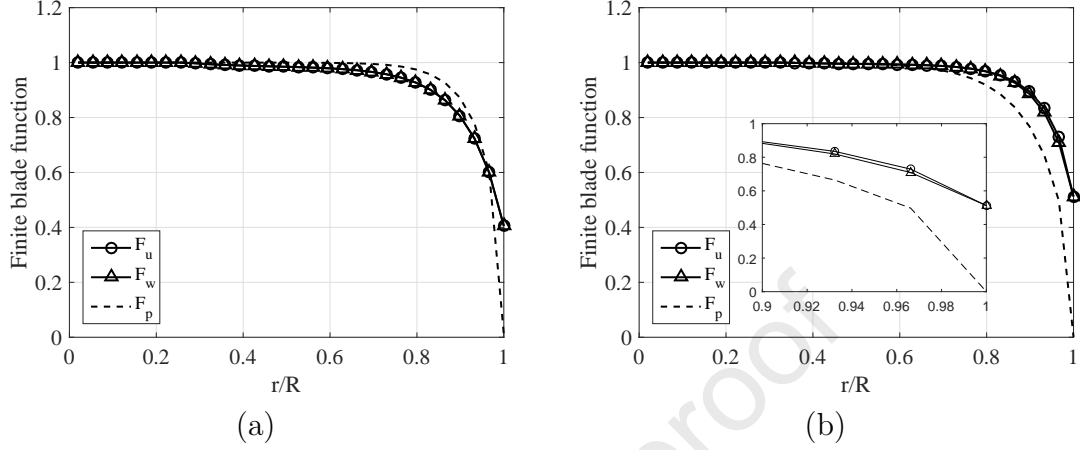
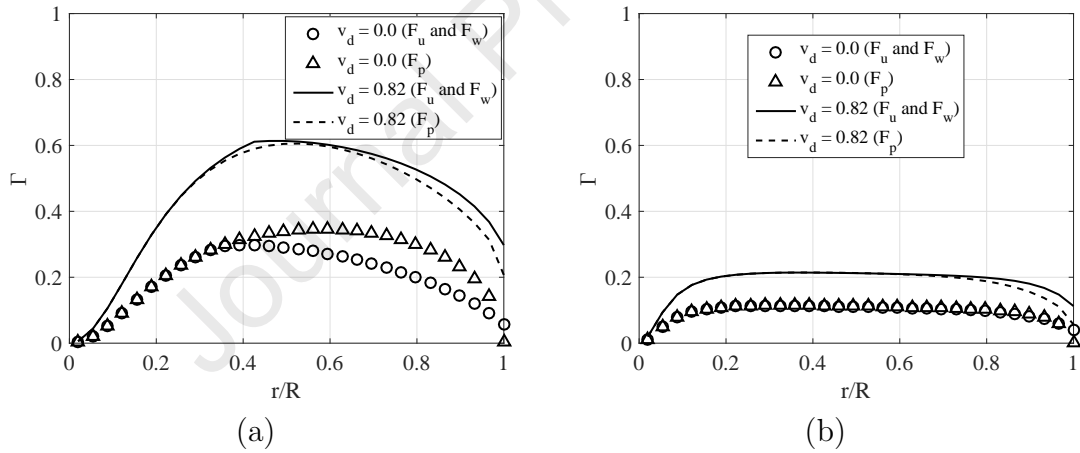


Figure 4: $\lambda = 2.0$: (a) $v_d = 0.0$ (b) $v_d = 0.82$.

Figure 5: $\lambda = 7.0$: (a) $v_d = 0.0$ (b) $v_d = 0.82$.Figure 6: (a) $\lambda = 2.0$. (b) $\lambda = 7.0$.

308 We now discuss the effect of the finite blade functions on the optimal
 309 c and θ distributions, which depend on them through Eqs. (32) and (33).
 310 From the results of the previous section, we expect the impact of using F_u
 311 and F_w in relation to F_P to be greater at the lower λ . Fig. 7a shows the
 312 chord and twist angle distributions for $\lambda = 2.0$. Using F_u and F_w , even for
 313 the bare turbine, gives a very different distribution of c to that using F_P ,
 314 while θ remains the same as for F_P , but sensitive to the diffuser as shown in
 315 Fig. 7b. At low λ , c from F_u and F_w is close to the Prandtl distribution,

316 being different only close to the blade tip. As the diffuser causes a finite v_d ,
 317 c near the tip remains slightly larger when using the finite blade functions,
 318 agreeing with the result in Fig. 4b, where F_u and F_w are directly affected
 319 by v_d . For $\lambda = 7.0$, Fig. 8a, c and θ are the same as that obtained using
 320 F_p . Even with the diffuser, Fig. 8b, c and θ distributions are only slightly
 321 different very close to the blade tip, but all of them are very sensitive to the
 322 diffuser. The optimized power extraction is listed in Table 3; using F_u and
 323 F_w the power is almost equal that using F_p for $\lambda = 2.0$. However, for $\lambda = 7.0$
 324 the power is about 6.6% higher than for F_p mainly because v_d increases F_u
 325 and F_w . These results demonstrate that to optimize DAWTs it is necessary
 326 to consider the axial induced velocity, v_d , of the diffuser, which alters the
 327 finite blade function mainly close to the tip.

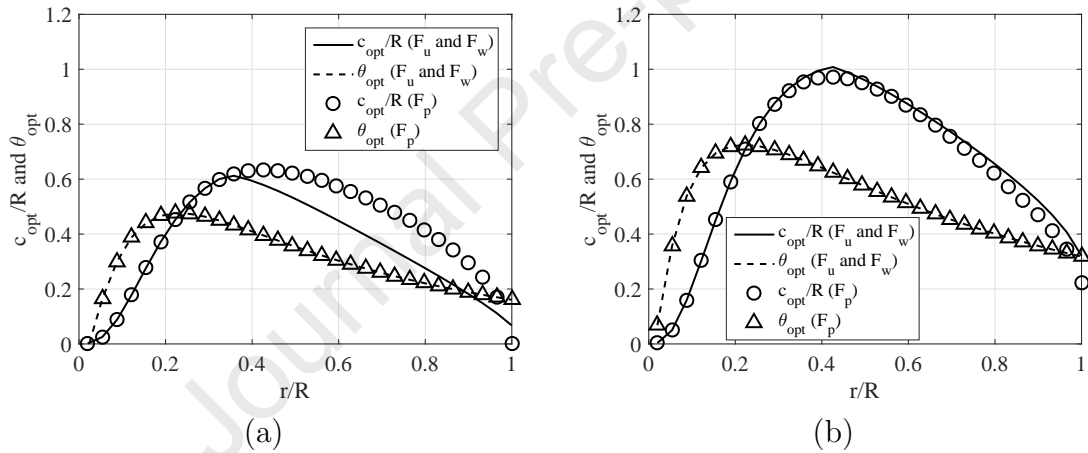
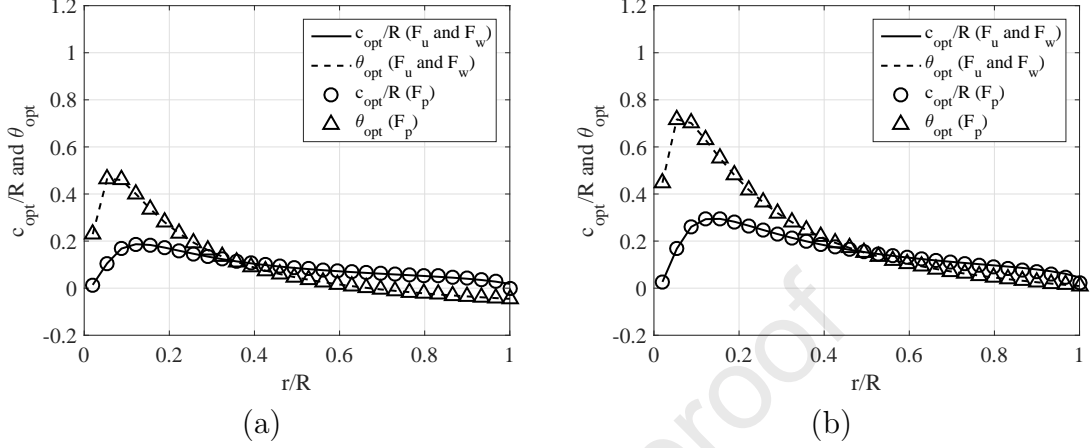


Figure 7: $\lambda = 2.0$: (a) $v_d = 0.0$ (b) $v_d = 0.82$.

Figure 8: $\lambda = 7.0$: (a) $v_d = 0.0$ (b) $v_d = 0.82$.Table 3: Comparison between optimized power coefficients ($v_d = 0.82$).

	$\lambda = 2.0$	$\lambda = 7.0$
C_P using F_p	0.63	0.76
C_P using F_u and F_w	0.64	0.81

328 We now compare the present analysis with the experimental data of
 329 Hoopen [48] for a 3-bladed DAWT of 1.5 m rotor diameter at $\lambda = 5.6$.
 330 [48] gives all parameters needed for the present simulation, making his work
 331 an important DAWT source. Table 4 shows the present results compared
 332 with Hoopen's measurements and other methods available in the literature.
 333 Note that the power output (530.04 W) obtained using F_u and F_w is close
 334 to the experimental value (531 W), while using F_p the difference is slightly
 335 larger. The same occurs with the turbine torque. The thrust on the rotor
 336 using F_u and F_w also shows good agreement with the measurements, as well
 337 as that value using F_p . Fig. 9a shows the behavior of F_u , F_w , and F_p for
 338 $V_0 = 10$ m/s. As $\lambda = 5.6$ in this case, F_u , F_w , and F_p are almost the same.
 339 Fig. 9b shows the augmentation factor, A_f , in relation to the wind velocity,
 340 V_0 . A_f is defined in [11]; $A_f = 27\eta_t/16$, with $\eta_t = \eta_p\eta_g C_P$, where $\eta_p = 0.85$
 341 is the drivetrain efficiency and $\eta_g = 0.74$ is the generator efficiency. The results
 342 in Fig. 9 were obtained for constant Ω , so $\lambda = 56/V_0$. Clearly, the results
 343 using F_u and F_w , and also F_p are consistent with the measurements. This
 344 occurs because to calculate F_u , F_w , and F_p it is necessary to include v_d in the

345 BEMT calculations. As before, the differences between F_P and F_u and F_w
 346 increase with decreasing λ . For the results in Fig. 9, $v_d = 0.85$, which was
 347 calculated for $c_{p3} = -0.49$, $\beta = 0.5785$ and $C_{Td} = 0.135$ as described in [48].

348 Fig. 9b suggest the intriguing possibility that maximum DAWT and
 349 DAHKT performance is much less dependent on λ than for a bare turbine.
 350 This would allow consideration of factors other than the maximization of
 351 power in turbine design. These other factors include: high λ performance
 352 usually allows more efficient and cheaper generators, but lower λ is likely
 353 to reduce cavitation in DAHKTs and the lower blade rotation would reduce
 354 the likelihood of damage to fish and other river life. Further, the high c/R
 355 shown in Fig. 7 implies high solidity and possibly higher lift:drag on the
 356 blade elements.

Table 4: Comparison between the present study and experimental data ($V_0 = 10\text{m/s}$).

	Angular speed (rad/s)	Power output (W)	Torque (Nm)	Thrust coefficient
Experimental [48]	75	531.00	7.10	0.80
Rio Vaz et al. [32]	75	526.00	6.10	-
Present work using F_p	75	536.26	7.15	0.77
Present work using F_u and F_w	75	530.04	7.07	0.77
CFD [48]	137	545.00	4.00	-
CFD [48]	155	246.00	1.60	-

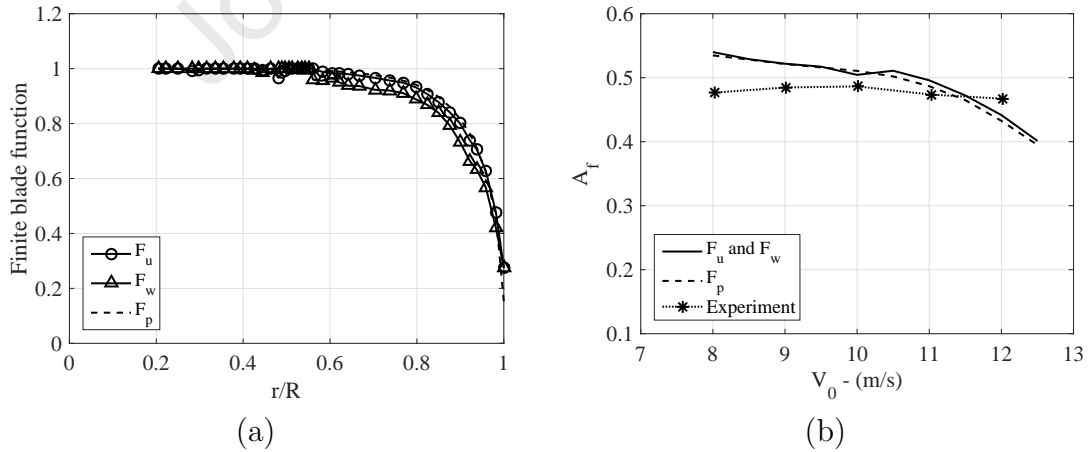


Figure 9: (a) Finite blade functions in relation to the radial position for $V_0 = 10$ m/s. (b) Augmentation factor in relation to V_0 (experiment obtained from [48]).

357 7. Conclusions

358 The present study considered an issue in blade element modeling of dif-
359 fuser augmented wind and hydrokinetic turbines that has not received suf-
360 ficient attention: the effects of the finite number of blades on the turbine
361 power and thrust. These are usually modeled by Prandtl's well-known tip
362 loss factor which asymptotes to zero at the blade tip. The diffuser, however,
363 induces an additional flow through the rotor causing finite blade loading at
364 the tip. Finite blade effects are measured by the ratio of the velocity at the
365 blade to the streamtube average. A diffuser has equal effect on the axial
366 velocities, so their ratio cannot reach zero. There is no corresponding con-
367 straint on the circumferential velocity, but F_w as well as F_u was found not
368 to go to zero at the tip.

369 F_u and F_w were modeled using a simple modification of the analysis of
370 Wood & Okulov [16] and Wood [19] for bare turbines to determine the finite
371 blade functions for the axial and circumferential velocities. As it is not clear
372 whether F_u and F_w can exceed unity, we limited the calculated values to
373 unity. This had only a small effect on the analysis because the exceedence
374 occurred only near the hub. The new analysis gave 6% increased power for
375 a computationally-optimized blade at the higher value of tip speed ratio of
376 the two that were analyzed.

377 By comparison to the limited experimental data for a diffuser-augmented
378 wind turbine, we could not distinguish between F_P and F_u and F_w in terms
379 of accuracy, as shown in Tab. 4. In addition, this work suggests that diffuser-
380 augmented wind turbines have much flatter power curves than bare turbines.
381 Some of the possible advantages of this behaviour were given. These results
382 show that the new finite blade functions can be implemented in BEMT anal-
383 ysis, in order to contribute for a more accurate BEMT model for DAWTs.

Nomenclature**Latin Symbols**

a, a'	Streamtube average axial and tangential induction factors
a_b, a'_b	Axial and tangential induction factors at the blade
A, A_3	Area of the disc and the cross section at the diffuser outlet
B	Number of blades
c	Chord (m)
C_D	Drag coefficient
C_L	Lift coefficient
C_M	Torque coefficient
C_n	Normal force coefficient
c_{p3}	Pressure coefficient at the diffuser outlet
C_P	Power coefficient
C_t	Tangential force coefficient
C_T	Thrust coefficient
C_{Td}	Diffuser thrust coefficient
dM	Elementary torque (Nm)
dP	Elementary power (W)
F	Prandtl Tip-loss factor
F_u, F_w	Finite blade functions for axial and circumferential flow, respectively
H	Losses through the diffuser in terms of pressure (Pa)
p_0	Pressure in the external flow (Pa)
p_2	Pressure at the turbine upstream (Pa)
p_3	Pressure at the diffuser outlet (Pa)
P	Power output (W)
Q	Flow rate (m ³ /s)
r	Radial position at the rotor plane (m)
R	Radius of the rotor (m)
T	Thrust of the rotor (N)
T_d	Thrust of the diffuser (N)
u_θ	Swirl velocity in the near wake (m/s)
V_0	Freestream wind velocity (m/s)
V_1, V_2	Axial velocity at the rotor (m/s)
V_3	Axial velocity at the diffuser outlet (m/s)
V_4	Axial velocity in the wake (m/s)
x	Local-speed ratio

Greek Symbols

α	Angle of attack (rad)
β	Area ratio
ε_1	Velocity ratio
ε_4	Far-wake velocity ratio
η_d	Diffuser efficiency
θ	Twist angle (rad)
λ	Tip-speed ratio

384 **Acknowledgments**

385 The contribution of VLO and DHW was supported by a contract with
386 the Ministry of Education and Science of the Russian Federation (no. 075-15-
387 2019-1923). JRPV thanks CNPq, CAPES, PROCAD project (no. 88881.200549/2018-
388 01), and PROPESP/UFGA for financial support.

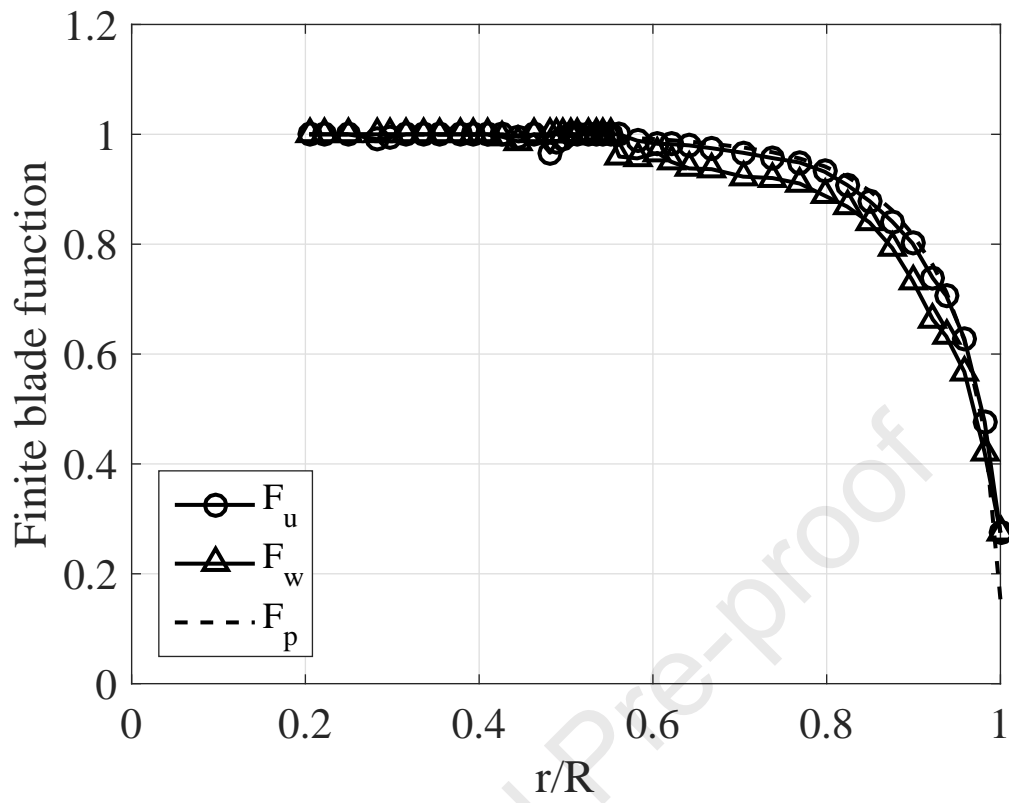
- 389 [1] Jamieson, P. Innovation in wind turbine design. John Wiley & Sons,
390 2018.
- 391 [2] Hansen, M.O.L.; Sorensen, N.N.; Flay, R.G.J. Effect of placing a diffuser
392 around a wind turbine. *Wind Energy* 2000; 3:207-213
- 393 [3] Hjort, S., Larsen, H. . A multi-element diffuser augmented wind turbine.
394 *Energies* 2015 7(5): 3256-3281.
- 395 [4] Anup, K. C., Whale, J., Urmee, T. Urban wind conditions and small
396 wind turbines in the built environment: A review. *Renewable Energy*
397 2018, 131:268-283.
- 398 [5] Dilimulati, A., Stathopoulos, T., Paraschivoiu, M. Wind turbine designs
399 for urban applications: A case study of shrouded diffuser casing for tur-
400 bines. *Journal of Wind Engineering and Industrial Aerodynamics* 2018,
401 175: 179-192.
- 402 [6] Silva, P. A., Vaz, D. A. R., Britto, V., de Oliveira, T. F., Vaz, J. R.,
403 Junior, A. C. B. A new approach for the design of diffuser-augmented
404 hydro turbines using the blade element momentum. *Energy Conversion*
405 and Management, 2018, 165, 801-814.
- 406 [7] Lubitz, W.D., Shomer, A. Wind loads and efficiency of a diffuser aug-
407 mented wind turbine, Proc. CSME Intl Congress, Toronto, 2014.
- 408 [8] Hansen, M.O.L., *The Aerodynamics of Wind Turbines*, 2nd edn, Earth-
409 scan.
- 410 [9] Kesby, J. E., D. R. Bradney, P. D. Clausen. Determining Diffuser
411 Augmented Wind Turbine performance using a combined CFD/BEM
412 method. *Journal of Physics: Conference Series*. 753(8). IOP Publishing,
413 2016.

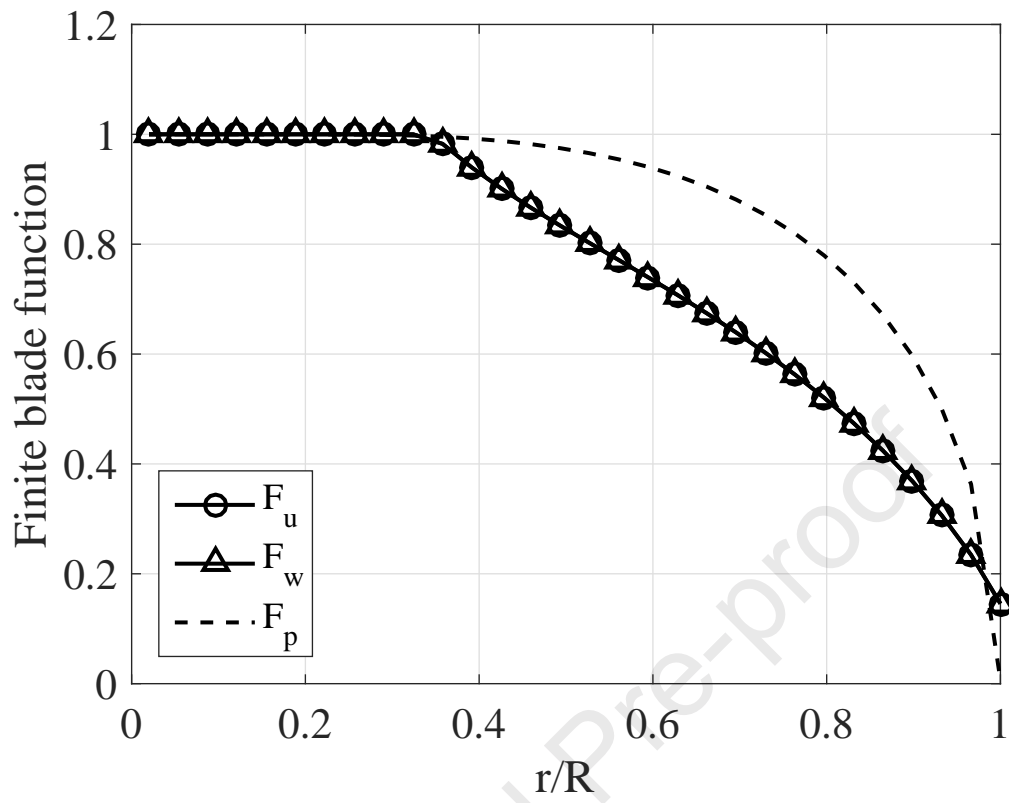
- 414 [10] Fletcher, C.A.J. Computational analysis of diffuser-augmented wind tur-
415 bines. *Energy Conversion Management* 1981; 21:175-183.
- 416 [11] Vaz, J.R.P., Wood, D.H., Effect of the diffuser efficiency on wind turbine
417 performance. *Renewable Energy* 2018, 126:969-977.
- 418 [12] Glauert H. Aerodynamic theory. In: Durand WF, editor. Chapter
419 XI. Division L. Airplanes Propellers, vol.4; 1935. p.191-195 [reprinted,
420 Dover, New York, 1963].
- 421 [13] Sørensen, J. N. General Momentum Theory for Horizontal Axis Wind
422 Turbines. *Research Topics in Wind Energy*, Vol. 4, Springer Interna-
423 tional Publishing, 2016 (DOI 10.1007/978-3-319-22114-4).
- 424 [14] Shen, W.Z., Mikkelsen, R., Sørensen, J.N., Bak, C..Tip vortex correc-
425 tions for wind turbine computations. *Wind Energy* 2005, 8:457-475.
- 426 [15] Wimhurst, A., and Willden, R. H. J.. Analysis of a tip correction factor
427 for horizontal axis turbines. *Wind Energy* 2017, 20,1515-1528.
- 428 [16] Wood, D. H. Application of extended vortex theory for blade element
429 analysis of horizontal-axis wind turbines. *Renewable Energy* 2018, 121:
430 188-194.
- 431 [17] Wood, D. H. A cascade model of blade element interaction for wind tur-
432 bines with unequal blades. *International Journal of Sustainable Energy*,
433 2016, 35(5): 502-512.
- 434 [18] Passmann M, aus der Wiesche S, Joos F. An Experimental and Numeri-
435 cal Study of Tip-Leakage Flows in an Idealized Turbine Tip Gap at High
436 Mach Numbers. In *Turbo Expo: Power for Land, Sea, and Air*, 2018,
437 51005, V02BT41A023. American Society of Mechanical Engineers.
- 438 [19] Wood, D.H., Okulov, V.L., Nonlinear blade element-momentum analysis
439 of Betz-Goldstein rotors, *Renewable Energy* 2017, 107:542-549.
- 440 [20] Okulov, V. L. On the stability of multiple helical vortices. *Journal of*
441 *Fluid Mechanics* 2004, 521: 319-342.
- 442 [21] Fukumoto, Y., Okulov, V. L., Wood, D. H. . The contribution of Kawada
443 to the analytical solution for the velocity induced by a helical vortex
444 filament. *Applied Mechanics Reviews* 2015, 67(6): 060801.

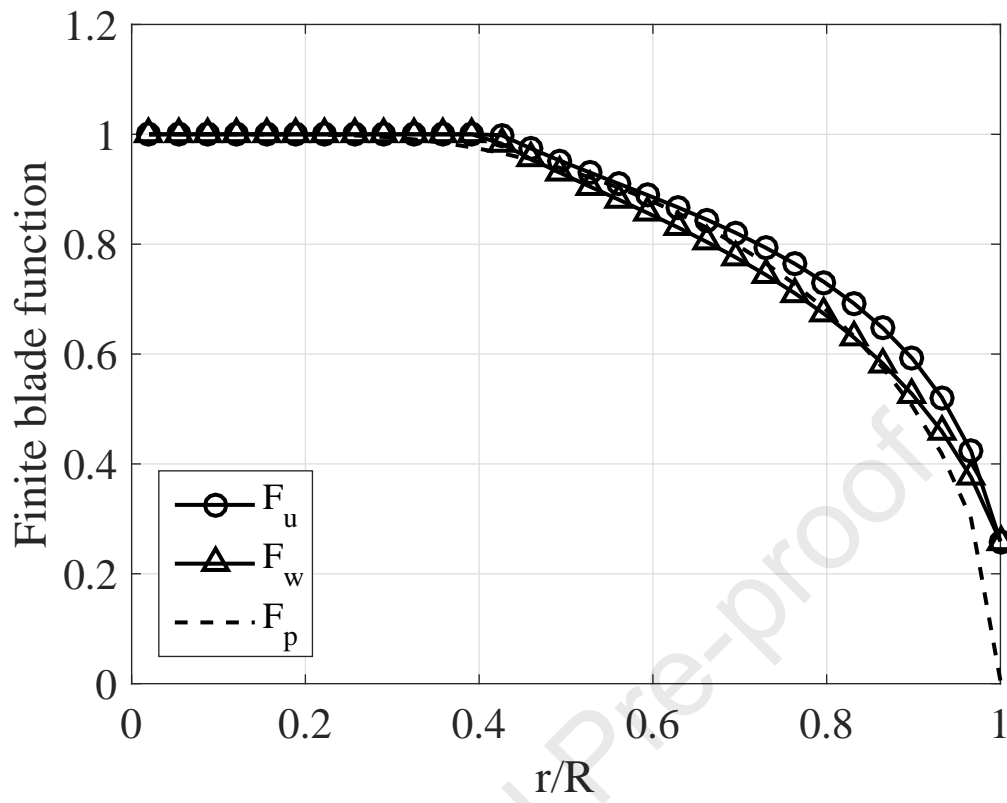
- 445 [22] Okulov, V.L., Sørensen, J.N., Refined Betz limit for rotors with a finite
446 number of blades. *Wind Energy* 2008, 11(4): 415-426.
- 447 [23] Sorribes-Palmer, F., Sanz-Andres, A., Ayuso, L., Sant, R., Franchini, S.,
448 Mixed CFD-1D wind turbine diffuser design optimization, *Renewable*
449 *Energy* 2017, 105:386-399.
- 450 [24] Kosasih, B., Hudin, H.S., Influence of inflow turbulence intensity on the
451 performance of bare and diffuser-augmented micro wind turbine model,
452 *Renewable Energy* 2016, 87:154-167.
- 453 [25] Bontempo, R., Manna, M., Performance analysis of open and ducted
454 wind turbines, *Applied Energy* 2014, 136:405-416.
- 455 [26] Vaz, J.R.P., Wood, D.H., Aerodynamic optimization of the blades of
456 diffuser-augmented wind turbines. *Energy Conversion and Management*
457 2016, 123:35-45.
- 458 [27] Al-Sulaiman, F. A., Yilbas, B. S., Thermoeconomic analysis of shrouded
459 wind turbines, *Energy Conversion and Management* 2015, 96:599-604.
- 460 [28] Jafari, S.A.H., Kosasih, B., Flow analysis of shrouded small wind tur-
461 bine with a simple frustum diffuser with computational fluid dynamics
462 simulations, *Journal of Wind Engineering and Industrial Aerodynamics*
463 2014, 125:102-110.
- 464 [29] Wang, W.X., Matsubara, T., Hu, J., Odahara, S., Nagai, T., Karasutani,
465 T., Ohya, Y., Experimental investigation into the influence of the flanged
466 diffuser on the dynamic behavior of CFRP blade of a shrouded wind
467 turbine, *Renewable Energy* 2015, 78:386-397.
- 468 [30] Abe, K.; Ohya, Y. An investigation of flow fields around flanged dif-
469 fusers using CFD, *Journal of Wind Engineering Industrial Aerodynam-*
470 *ics* 2004;. 92: 315-330.
- 471 [31] Ohya, Y.; Karasudani, T. A shrouded wind turbine generating high
472 output power with wind-lens technology, *Energies* 2010; 3:634-649.
- 473 [32] Rio Vaz, D. A. T. D., Mesquita, A. L. A., Vaz, J. R. P., Blanco, C. J.
474 C., Pinho, J. T., An extension of the Blade Element Momentum method
475 applied to Diffuser Augmented Wind Turbines, *Energy Conversion and*
476 *Management* 2014, 87:1116-1123.

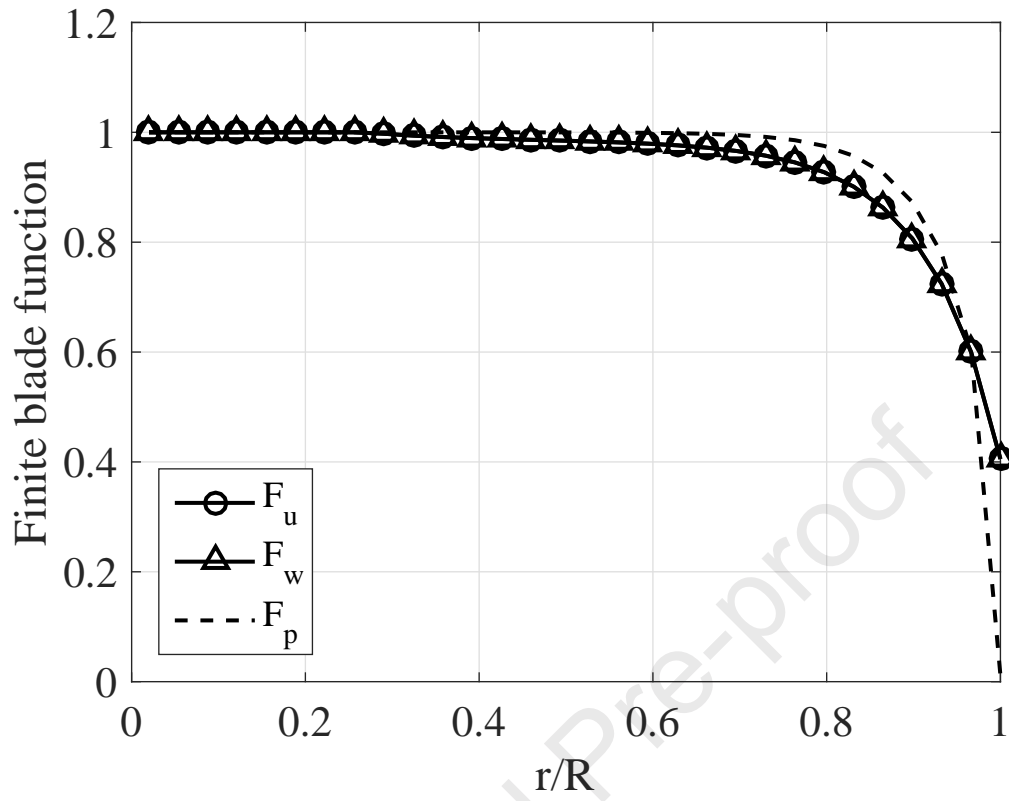
- 477 [33] Igra, O. Research and development for shrouded wind turbines. *Energy*
478 *Conversion Management* 1981; 21: 13-48.
- 479 [34] Batchelor, G.K. *An Introduction to Fluid Dynamics*, C.U.P., 1967.
- 480 [35] Clausen, P.D., Koh, S.G., and Wood, D.H. (1993). Measurements of a
481 turbulent boundary layer developing in a conical diffuser, *Experimental*
482 *Thermal and Fluid Science*, 1993, 6: 39 - 48.
- 483 [36] Spera, D. A. *Wind Turbine Technology: fundamental concepts of wind*
484 *turbine engineering*. ASME Press, 2nd Ed., New York, 2009.
- 485 [37] Wilson, R. E., and S. N. Walker, *Performance Analysis of Horizontal*
486 *Axis Wind Turbines*, Corvallis 1984, Oregon: Oregon State University.
- 487 [38] Moriarty P.J., Hansen A.C. *Aerodyn theory manual*. Tech. Rep.
488 NREL/TP 500-36881. Golden, CO: National Renewable Energy Lab-
489 oratory; 2005.
- 490 [39] van Bussel, G.J.W. An assessment of the performance of diffuser aug-
491 mented wind turbines (DAWT's). 3th ASME/JSME Joint Fluids Engi-
492 neering Conference, July 18-23, San Francisco, California, USA; 1999.
- 493 [40] Phillips, D.G. An investigation on diffuser augmented wind turbine de-
494 sign, PhD. thesis, Department of Mechanical Engineering, School of
495 Engineering, The University of Auckland; 2003.
- 496 [41] Hansen, M. *Aerodynamics of wind turbines*. Earthscan 2nd ed.; 2008.
- 497 [42] Wilson, R. E., Lissaman, P. B. S. *Applied Aerodynamics of Wind Power*
498 *Machines*, Corvallis, Oregon: Oregon State University, 1974.
- 499 [43] Clifton-Smith, M. J., *Wind Turbine Blade Optimisation with Tip Loss*
500 *Corrections*, *Wind Engineering*, 2009, 33(5):477496.
- 501 [44] Buhl, M. L., *A New Empirical Relationship Between Thrust Coefficient*
502 *and Induction Factor for the Turbulent Windmill State*, Technical Re-
503 port NREL/TP-500-36834, August 2005.
- 504 [45] Lock, C.N.H.; Batemen, H.; Townsend, H.C.H. (1926). *An Extension of*
505 *the Vortex Theory of Airscrews with Applications to Airscrews of Small*
506 *Pitch, Including Experimental Results*. No. 1014. Aeronautical Research

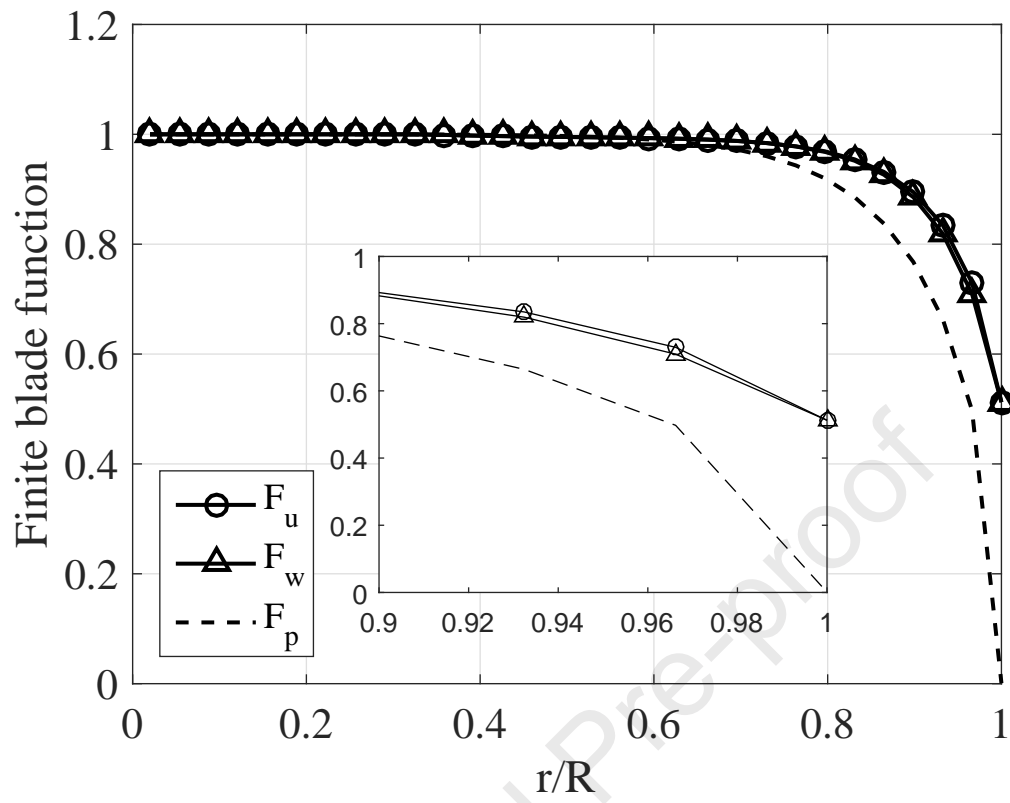
- 507 Committee Reports and Memoranda, London: Her Majesty's Stationery
508 Office.
- 509 [46] Barbosa, D.L.M., Vaz, J.R.P., Figueiredo, S.W.O., Silva, M.O., Lins,
510 E.F., Mesquita, A.L.A, An Investigation of a Mathematical Model for
511 the Internal Velocity Profile of Conical Diffusers Applied to DAWTs,
512 Annals of the Brazilian Academy of Sciences 2015, Vol. 87, No. 2,
513 <http://dx.doi.org/10.1590/0001-3765201520140114>.
- 514 [47] Bontempo, R., Manna, M., Effects of the duct thrust on the performance
515 of ducted wind turbines, *Energy*, 2016, 99:274-287.
- 516 [48] Hoopen P. D. C. An experimental and computational investigation of a
517 diffuser augmented wind turbine: with an application of vortex gener-
518 ators on the diffuser trailing edge, M.Sc. Thesis. Faculty of Aerospace
519 Engineering, Delft University of Technology; 2009.
- 520 [49] National Aerospace Laboratory (NLR). Evaluatie en verbetering van
521 de prestaties van eenkleinschalige diffuser augmented wind turbine
522 (DAWT); 1e fase; 2008.
- 523 [50] Sheldahl R, Klimas P. Aerodynamic characteristics of seven symmetrical
524 airfoil sections through 180-degree angle of attack for use in aerodynamic
525 analysis of vertical axis wind turbines. Sandia National Laboratories;
526 1981. Report SAND80-2114.
- 527 [51] Wood, D.H., Okulov, V.L. , Bhattacharjee, D., Direct calculation of
528 wind turbine tip loss, *Renewable Energy* 2016, 95:269-276.

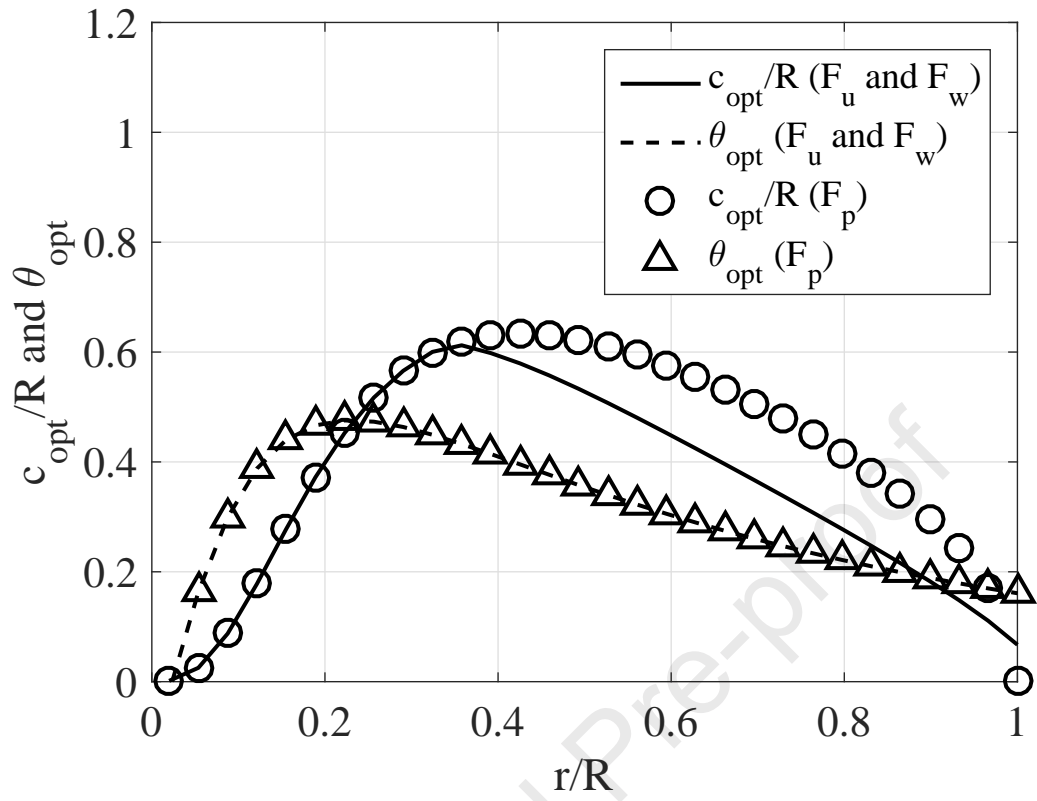


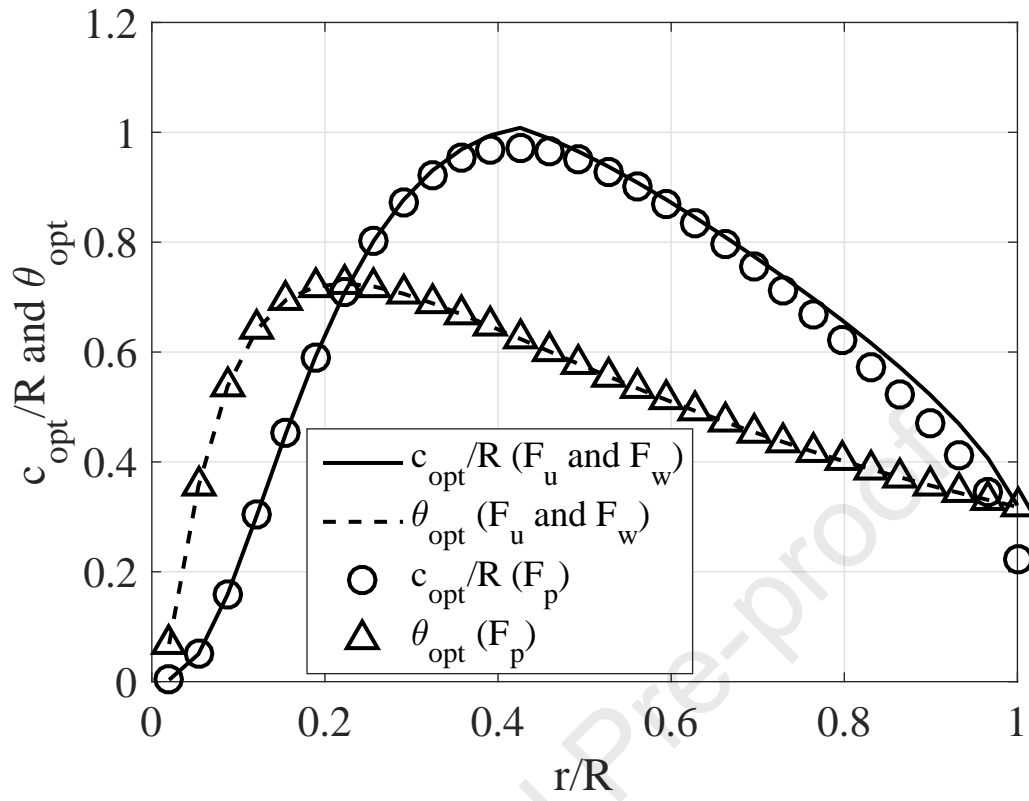


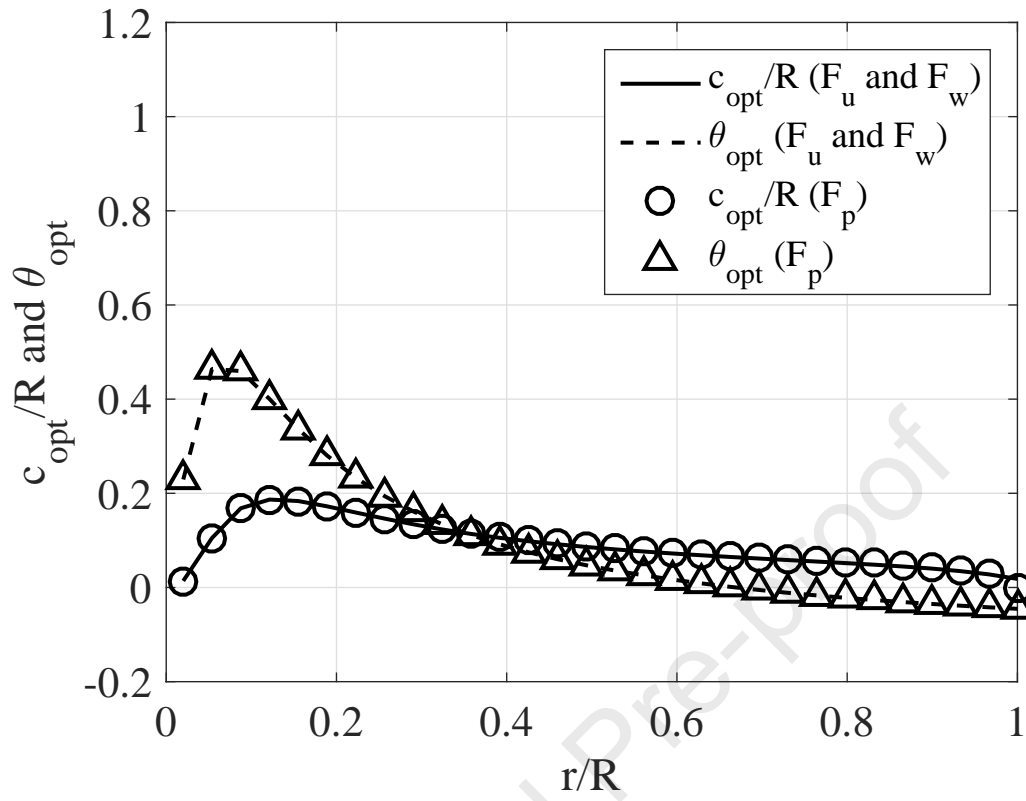


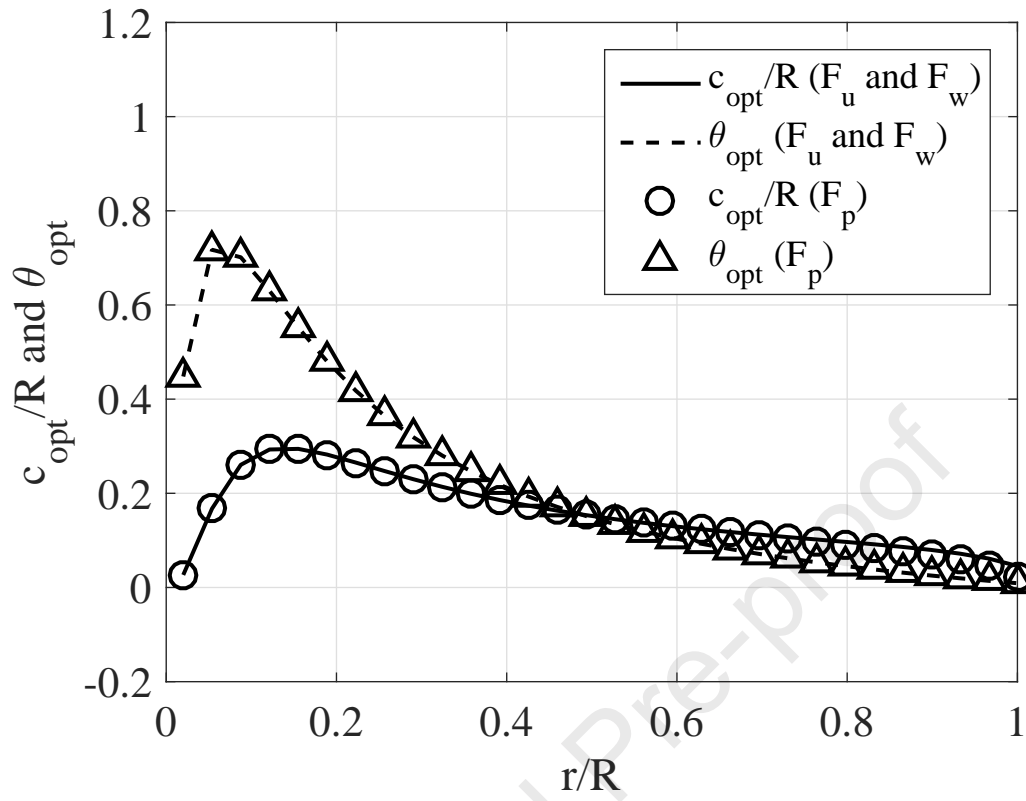


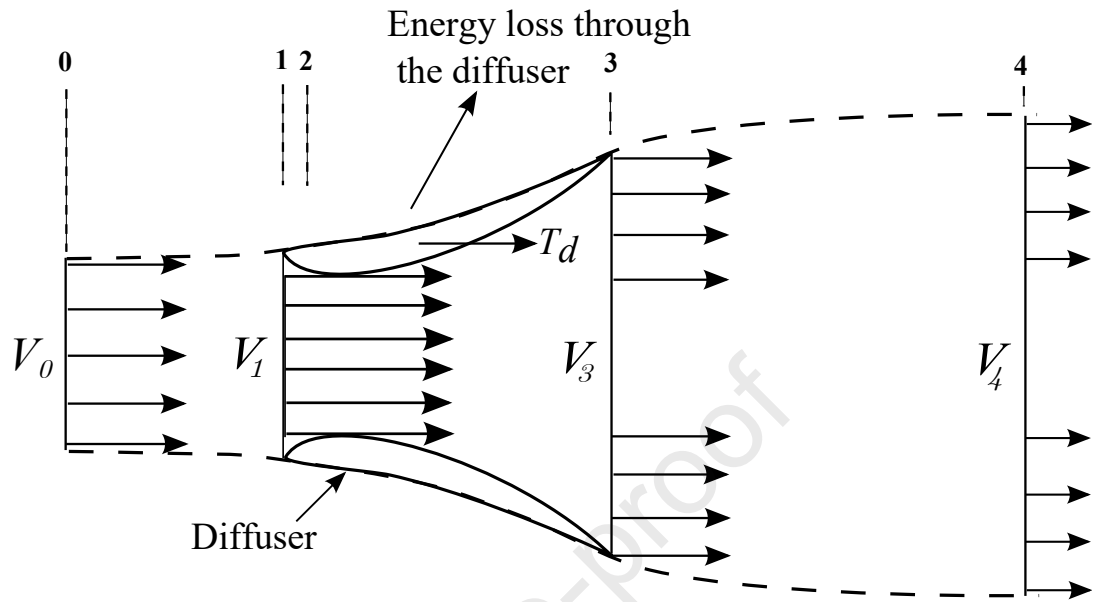


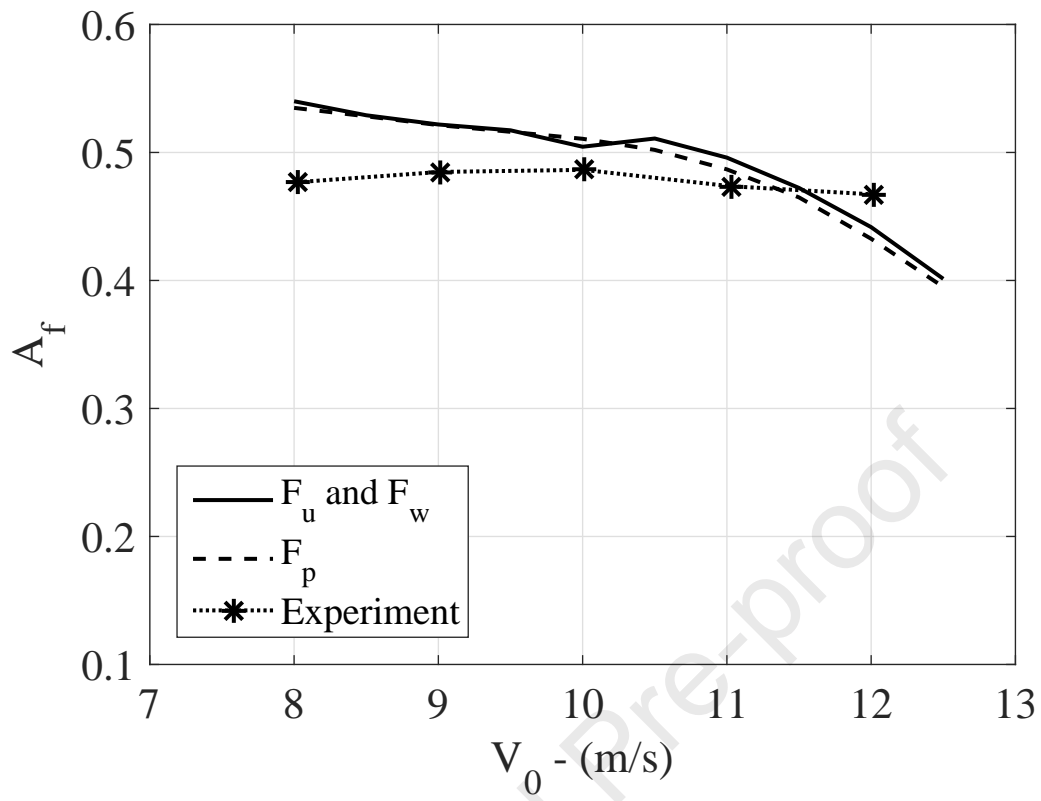


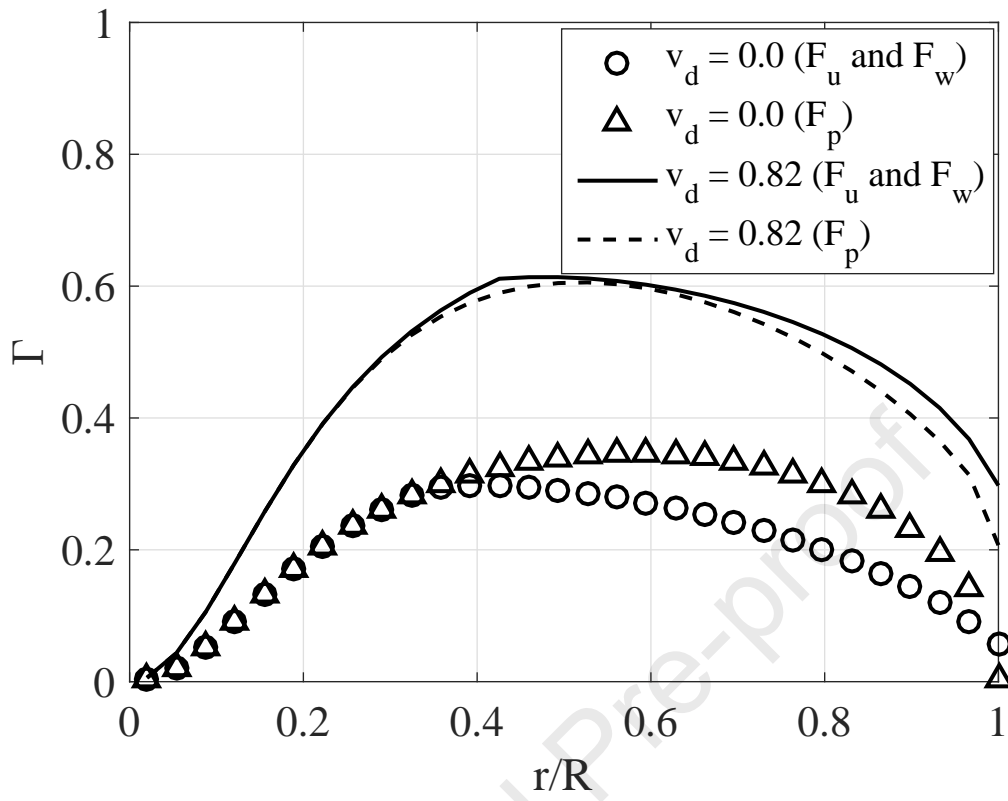


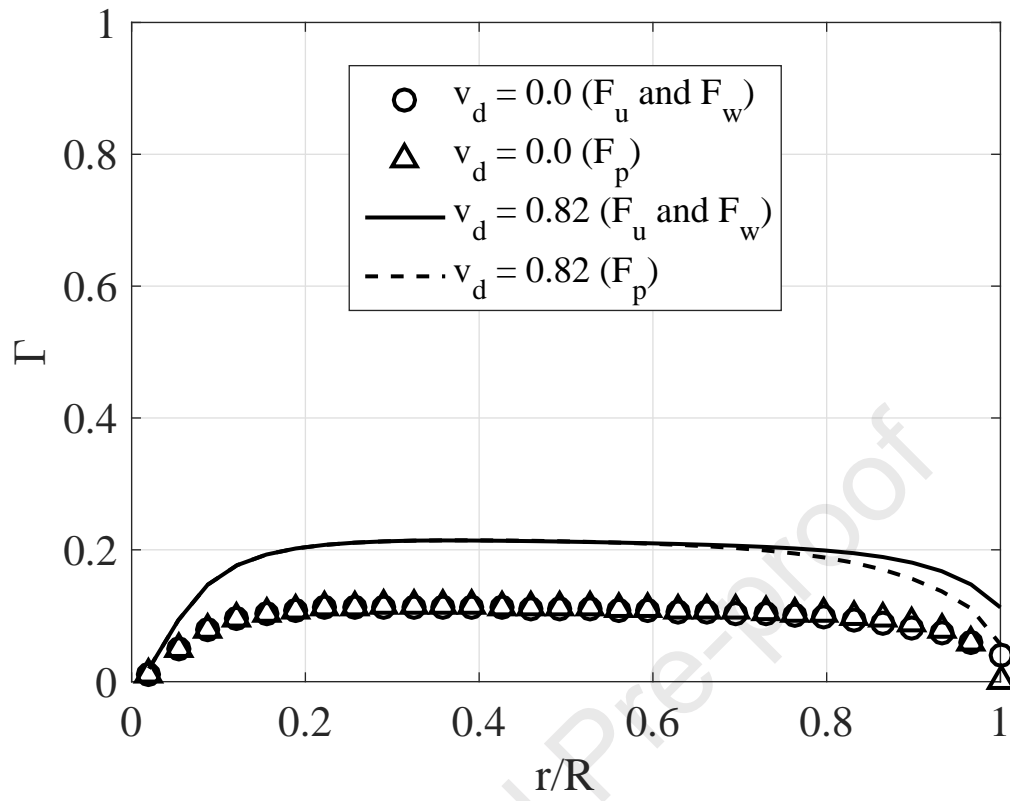


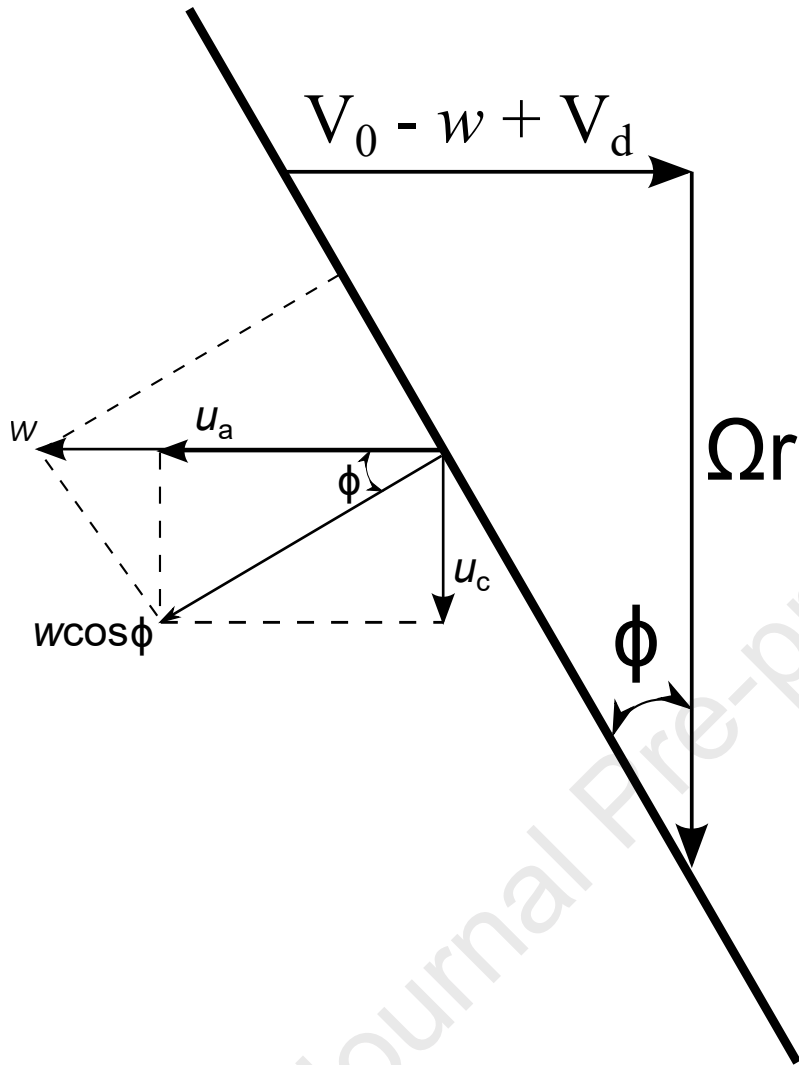


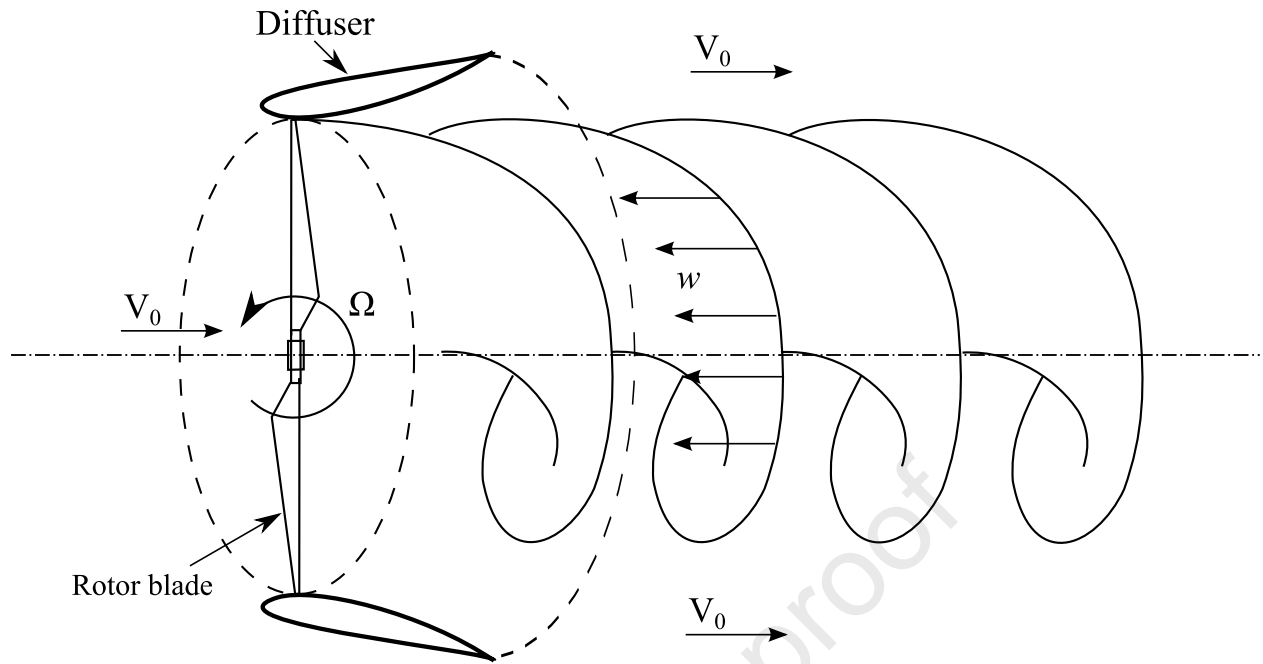












Highlights

- A new model for the finite number of blades in diffuser-augmented wind turbines;
- The blade loading is finite at the tip in contrast to bare turbines;
- Finite blade functions to optimize chord and twist angle of shrouded blades;
- Diffuser-augmented turbine power output seems to be less sensitive to tip speed ratio;
- Good agreement is demonstrated with available experiments.

Journal Pre-proof

Declaration of interests

The authors declare that they have no known competing financial interests or personal relationships that could have appeared to influence the work reported in this paper.

The authors declare the following financial interests/personal relationships which may be considered as potential competing interests:

The authors declare no conflicts of interest.

Journal Pre-proof